nature photonics

ARTICLES

PUBLISHED ONLINE: 25 MAY 2015 | DOI: 10.1038/NPHOTON.2015.84

Efficient inverted polymer solar cells employing favourable molecular orientation

Varun Vohra[1*†], Kazuaki Kawashima[2,3], Takeshi Kakara[3], Tomoyuki Koganezawa[4], Itaru Osaka[2,5*], Kazuo Takimiya[2*] and Hideyuki Murata[1*]

Improving the power conversion efficiency of polymer-based bulk-heterojunction solar cells is a critical issue. Here, we show that high efficiencies of ~10% can be obtained using the crystalline polymer PNTz4T in single-junction inverted cells with a thick active layer having a thickness of ~300 nm. The improved performance is probably due to the large population of polymer crystallites with a face-on orientation and the 'favourable' distribution of edge-on and face-on crystallites along the film thickness (revealed by in-depth studies of the blend films using grazing-incidence wide-angle X-ray diffraction), which results in a reduction in charge recombination and efficient charge transport. These results underscore the great promise of polymer solar cells and raise the hope of achieving even higher efficiencies by means of materials development and control of molecular ordering.

The bulk-heterojunction (BHJ) solar cell consisting of semiconducting polymers and fullerene derivatives as the p-type (hole transport or electron donor) and n-type (electron transport or electron acceptor) materials, respectively, is an emerging device that can enable lightweight, large-area, flexible, low-cost and low-energy fabrication, in contrast to silicon technology[1–3]. Although the power conversion efficiencies (PCE) of such polymer-based BHJ solar cells (PSCs) have improved rapidly in the last decade, exceeding 9% in single-junction cells[4–7] and reaching a milestone value of 10% in tandem cells[8,9], improving the PCE remains a formidable challenge.

As has been demonstrated in earlier studies on PSCs, the development of semiconducting polymers with alternating electron-rich (donor, D) and electron-poor (acceptor, A) building units (that is, D–A polymers) is key to improving PCE values[10–13]. D–A polymers afford absorption bands in the long-wavelength region (that is, a small bandgap) due to orbital mixing between the D and A units, which produces a large short-circuit current (J_{SC}) in PSCs. In line with this design strategy, numerous D–A semiconducting polymers have been synthesized. Examples of pioneering works include a cyclopentadithiophene–benzothiadiazole polymer (PCPDTBT)[14,15], a carbazole–benzothiadiazole polymer (PCDTBT)[16,17], and a series of benzodithiophene–thienothiophene polymers (PTBs)[18–20].

We have previously reported a new D–A polymer with quaterthiophene and naphtho[1,2-*c*:5,6-*c*′]bis[1,2,5]thiadiazole (NTz)[21,22] as the D and A units, respectively (PNTz4T, Fig. 1). This polymer is promising, as it shows a high PCE of 6.3% in single-junction PSCs with [6,6]-phenyl-C_{61}-butyric acid methyl ester ($PC_{61}BM$) as the n-type material, thanks to its long-wavelength absorption in the range of 300–800 nm and a relatively large ionization potential of 5.15 eV (ref. 23). Another striking feature of PNTz4T is that it forms a crystalline structure with a lamellar motif in which the polymer backbones are π-stacked with a stacking distance of ~3.5 Å in the thin film. This π–π stacking distance is short compared with that of typical high-performance D–A polymers used in PSCs[24,25], owing to the strong intermolecular interactions most probably originating in the NTz-based backbone structure. In addition, PNTz4T forms a 'face-on' orientation in the polymer/$PC_{61}BM$ blend film, which is favourable for PSCs, but forms an 'edge-on' orientation in the polymer neat film that is suitable for transistors, in which high field-effect hole mobilities of up to 0.5 $cm^2\ V^{-1}\ s^{-1}$ have been observed. The high crystallinity and the favourable backbone orientation explain well the high photovoltaic performance of PNTz4T. Here, we demonstrate, as a result of further studies on PNTz4T, that a PCE of 10% has been achieved in a single-junction PSC with an inverted architecture and an active layer thickness of ~300 nm, which is much larger than PCEs of typical PSCs. Importantly, we have found that the face-on orientation is more abundant and that the distribution of the edge-on/face-on orientation through the film thickness is

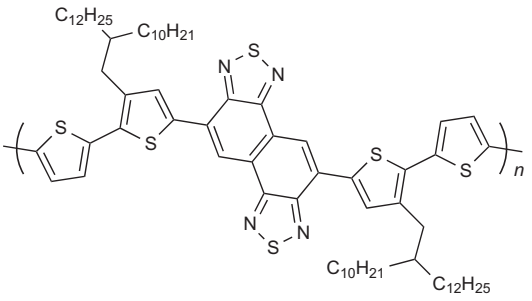

PNTz4T

Figure 1 | Chemical structure of PNTz4T, a quaterthiophene–naphthobisthiadiazole (NTz) copolymer.

[1]School of Materials Science, Japan Advanced Institute of Science and Technology (JAIST), 1-1 Asahidai, Nomi, Ishikawa 923-1292, Japan. [2]Emergent Molecular Function Research Group, RIKEN Center for Emergent Matter Science (CEMS), Wako, Saitama 351-0198, Japan. [3]Department of Applied Chemistry, Graduate School of Engineering, Hiroshima University, 1-4-1 Kagamiyama, Higashi-Hiroshima, Hiroshima 739-8527, Japan. [4]Japan Synchrotron Radiation Research Institute, 1-1-1 Kouto, Sayo-cho, Sayo-gun, Hyogo 679-5198, Japan. [5]Precursory Research for Embryonic Science and Technology, Japan Science and Technology Agency, Chiyoda-ku, Tokyo 102-0075, Japan. †Present address: Department of Engineering Science, Graduate School of Informatics and Engineering, The University of Electro-Communications (UEC), 1-5-1 Chofugaoka, Chofu-shi, Tokyo 182-8585, Japan.
*e-mail: varun.vohra@uec.ac.jp; itaru.osaka@riken.jp; takimiya@riken.jp; murata-h@jaist.ac.jp

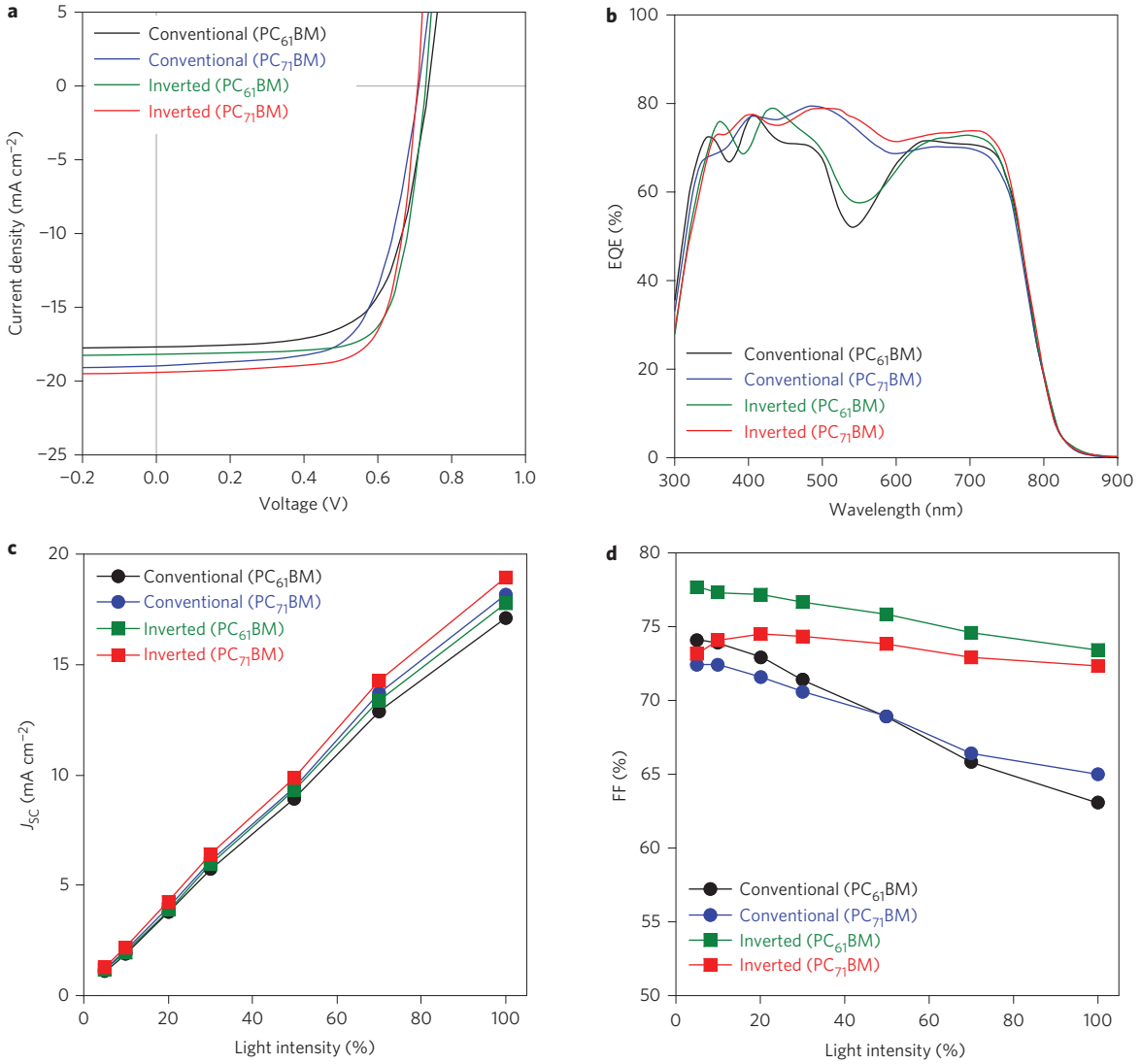

Figure 2 | Photovoltaic characteristics of PNTz4T-based cells with conventional and inverted architectures. a,b, *J*–*V* curves (**a**) and EQE spectra (**b**) of the best cells. **c**,**d**, J_{SC} (**c**) and FF (**d**) as a function of light intensity. Conventional architectures used are ITO/PEDOT:PSS/PNTz4T:$PC_{61}BM$ or $PC_{71}BM$/LiF/Al. Inverted architectures used are ITO/ZnO/PNTz4T:$PC_{61}BM$ or $PC_{71}BM$/MoO_x/Ag.

more favourable in the inverted cell than in the conventional cell, which should be key factors for understanding the origin of the high performance in PNTz4T cells.

Solar cell fabrications and performance

Solar cells with conventional and inverted architectures were fabricated. The cells were composed of indium tin oxide (ITO)/poly(3,4-ethylenedioxythiophene):polystyrene sulphonate (PEDOT:PSS)/PNTz4T:$PC_{61}BM$ or [6,6]-phenyl-C_{71}-butyric acid methyl ester ($PC_{71}BM$)/LiF/Al and ITO/ZnO/PNTz4T:$PC_{61}BM$ or $PC_{71}BM$/MoO_x/Ag, respectively. The PNTz4T to PCBM weight ratio was 1:2 in all cases. The active layer was fabricated by spin-coating the polymer/PCBM blend solution in *o*-dichlorobenzene (DCB). Note that no solvent additives were used in this system (for example, 1,8-diiodooctane (DIO) is often used to promote phase separation).

In a conventional cell using $PC_{61}BM$, a PCE of 6.55% with a J_{SC} of 12.1 mA cm^{-2}, an open-circuit voltage (V_{OC}) of 0.746 V and a fill factor (FF) of 72.7% were obtained with an active layer thickness of 150 nm (Supplementary Fig. 1 and Supplementary Table 1). This observed FF is fairly high considering that the active layer is 1.5 to 2 times thicker than that of typical PSCs (70–100 nm). We then fabricated cells with even thicker active layers (Supplementary Fig. 1 and Supplementary Table 1). Similarly to previous studies using thicker active layers[26–30], the value of J_{SC} increased with increasing thickness. V_{OC} decreased slightly with increasing thickness, but the change was relatively small. Although the FF showed a gradual decrease, it remained moderately high (66.7% at 300 nm). As a result, the overall PCE reached 8.70% with a J_{SC} of 17.7 mA cm^{-2} and V_{OC} of 0.738 V at 300 nm (Fig. 2a and Table 1). The external quantum efficiency (EQE) was generally high, at 70% in the polymer absorption ranges of 300–500 nm and 600–800 nm (Fig. 2b). In the conventional cell using $PC_{71}BM$, a large J_{SC} was obtained compared with the cell using $PC_{61}BM$ (Fig. 2a), which is due to the increased absorption and thus the high EQE in the range of 500–600 nm (Fig. 2b), as commonly observed for PSCs. The $PC_{71}BM$ cells showed a dependence of the photovoltaic parameters on the active layer thickness (Supplementary Fig. 2 and Supplementary Table 2), similarly to the $PC_{61}BM$ cell, and gave the highest PCE of 8.92% with the 290-nm-thick active layer (Table 1).

Interestingly, the inverted cells demonstrated high photovoltaic performances compared to the conventional cells, in particular in terms of J_{SC} and FF, as has been observed in other polymer systems (Fig. 2a,b and Table 1)[4,31,32]. The inverted cells also

Table 1 | Photovoltaic parameters of the best PNTz4T solar cells.

Cell structure	PCBM	Thickness (nm)	J_{SC} (mA cm^{-2})	V_{OC} (V)	FF (%)	PCE_{max} [PCE_{ave}] (%)
Conventional	$PC_{61}BM$	300	17.7	0.738	66.7	8.70 [8.46]
	$PC_{71}BM$	290	18.9	0.712	66.2	8.92 [8.65]
Inverted	$PC_{61}BM$	280	18.2	0.729	73.9	9.80 [9.55]
	$PC_{71}BM$	290	19.4	0.708	73.4	10.1 [9.77]

'Thickness' indicates active layer thickness; PCE_{max}, maximum power conversion efficiency; PCE_{ave}, average power conversion efficiency; J_{SC}, short-circuit current; V_{OC}, open-circuit voltage; FF, fill-factor.

showed the thickness dependence of photovoltaic performance (Supplementary Figs 3 and 4 and Supplementary Tables 3 and 4). Notably, the PCE reached 10.1% (J_{SC} = 19.4 mA cm^{-2}, V_{OC} = 0.708 V, FF = 73.4%), with an average of 9.77%, for the inverted $PC_{71}BM$ cell with an active layer thickness of ~290 nm, which is one of the highest PCEs observed in a single-junction cell. It is interesting to note that PCEs close to 10% were also observed for the inverted $PC_{61}BM$ cell with a thickness of 280 nm (PCE = 9.80% (average 9.55%), J_{SC} = 18.2 mA cm^{-2}, V_{OC} = 0.729 V, FF = 73.9%).

To investigate the reason for the higher FF in the inverted cell than in conventional cells, we conducted a qualitative study on the difference in charge recombination between the two device architectures by plotting J_{SC} and FF as a function of light intensity (Fig. 2c,d)[33]. It is clear that for both conventional and inverted $PC_{61}BM$ and $PC_{71}BM$ cells, J_{SC} increases linearly as the light intensity increases, wherein the number of free carriers increases. The decrease in FF with increasing light intensity was milder in the inverted cells than in conventional cells. The difference in the decrease in FF implies that bimolecular recombination is reduced in the inverted cell compared with the conventional cell, which may be one of the reasons for the higher FF in the inverted cell of this system.

Charge transport property

Charge carrier mobilities of the blend films in the direction perpendicular to the substrate plane were evaluated by using hole-only (ITO/PEDOT:PSS/active layer/MoO_x/Ag) and electron-only (ITO/ZnO/active layer/LiF/Al) devices (Supplementary Figs 8 and 9). The polymer neat film was also evaluated in the hole-only device (Supplementary Fig. 8). Both hole (μ_h) and electron (μ_e) mobilities were obtained using the space-charge limited current model. The value of μ_h for the polymer neat film was 7.2×10^{-4} cm^2 V^{-1} s^{-1}, while those for the blend films with $PC_{61}BM$ and $PC_{71}BM$ were 2.1×10^{-3} cm^2 V^{-1} s^{-1} and 3.4×10^{-3} cm^2 V^{-1} s^{-1}, respectively. The higher μ_h for the blend film than for the polymer neat film is probably due to the more favourable backbone orientation for vertical charge transport in the blends[23]. The μ_h values for the blends are fairly high for the semiconducting polymers[19] and most probably originate from the combination of the highly crystalline structure and short π–π stacking distance (3.5 Å), and the favourable face-on orientation. It should be noted that μ_e was also on the order of 10^{-3} cm^2 V^{-1} s^{-1} (2.3×10^{-3} cm^2 V^{-1} s^{-1} for the blend film with $PC_{61}BM$, and 1.1×10^{-3} cm^2 V^{-1} s^{-1} for that with $PC_{71}BM$). These results are indicative of the well-balanced hole and electron transport in the PNTz4T/PCBM blend films, explaining the high photovoltaic performance for the PNTz4T cells.

GIWAXD studies

The polymer microstructures in the blend films were studied by grazing-incidence wide-angle X-ray diffraction (GIWAXD) measurements. Figure 3a,b displays the two-dimensional GIWAXD images of PNTz4T/$PC_{61}BM$ blend films spun on ITO/PEDOT:PSS and ITO/ZnO substrates (film thickness, ~250 nm). In both cases, a diffraction corresponding to the π–π stacking appeared only along the q_z axis (out-of-plane direction), suggesting that there is a large population of polymer crystallites with the face-on orientation[34]. Nevertheless, diffractions corresponding to the lamellar structure appeared along both the q_z and q_{xy} (in-plane direction) axes, indicating that edge-on and face-on crystallites co-exist in the film. These results indicate that the polymer easily forms a crystalline structure in the blend films by spin-coating from DCB solution onto both substrates. The fact that PNTz4T/$PC_{71}BM$ blend films also showed similar textures to the PNTz4T/$PC_{61}BM$ blend films (Supplementary Fig. 11) suggests that there is no significant difference in polymer crystallinity and orientation between the $PC_{61}BM$ and $PC_{71}BM$ blend films.

To gain a deeper insight into the orientation, we performed a pole figure analysis of the blend films[35,36]. Figure 3c shows the pole figures extracted from the lamellar diffraction, (100), of PNTz4T in the two-dimensional GIWAXD patterns for the PNTz4T/$PC_{61}BM$ blend films on the ITO/PEDOT:PSS and ITO/ZnO substrates (thickness, ~250 nm), as shown in Fig. 3a,b (see insets for a close-up of the lamellar diffraction). We defined the areas integrated with polar angle χ ranges of 0–45° and 135–180° (A_{xy}) and 55–125° (A_z) as those corresponding to the fractions of face-on and edge-on crystallites, respectively. It is interesting to note that the ratio of A_{xy} to A_z (A_{xy}/A_z) for the blend film on the ITO/ZnO substrate was 0.79, which was higher than that for the blend film on the ITO/PEDOT:PSS substrate, namely 0.64. This means that the population of the face-on crystallite is larger in the inverted cells than in the conventional cells. This could be attributed to the difference in wettability of the solution on the substrate surfaces. It has been reported that substrate surfaces with lower wettability induce a higher tendency for edge-on orientation to semiconducting polymers in the thin film by spin-coating the polymer solution[37]. We therefore measured the contact angle of DCB, the solvent used for spin-coating, on the PEDOT:PSS and ZnO surfaces (both coated on the ITO glass substrate), and obtained average values of 18.5° and 6.1°, respectively (Supplementary Fig. 19). This suggests that the PEDOT:PSS surface has low wettability compared to the ZnO surface, which may explain the larger population of edge-on orientation on the PEDOT:PSS surface (and larger population of face-on orientation on the ZnO surface).

We also carried out pole figure analysis of the PNTz4T/$PC_{61}BM$ blend films on ITO/PEDOT:PSS and ITO/ZnO substrates with different thicknesses ranging from ~50 nm to 400 nm (Supplementary Figs 12, 13 and 16), then plotted A_{xy}/A_z as a function of film thickness (Fig. 3d). For all thicknesses, A_{xy}/A_z was larger for the ITO/ZnO substrate than for the ITO/PEDOT:PSS substrate. Notably, A_{xy}/A_z increased gradually with increasing film thickness in both cases; that is, the population of the face-on crystallites increased with film thickness. This suggests that the face-on to edge-on ratio is not distributed evenly along the film thickness. One can assume that the orientation in the interfacial layers at the bottom (PEDOT:PSS or ZnO) and top (air), as well as the thickness of the interfacial layer, is independent of the total film thickness. Thus, this increase in the face-on crystallite population mainly occurs at the bulk, and arises from the increase in the bulk volume in thicker films. This means that the edge-on crystallites are abundant either at the film–bottom or film–air interface.

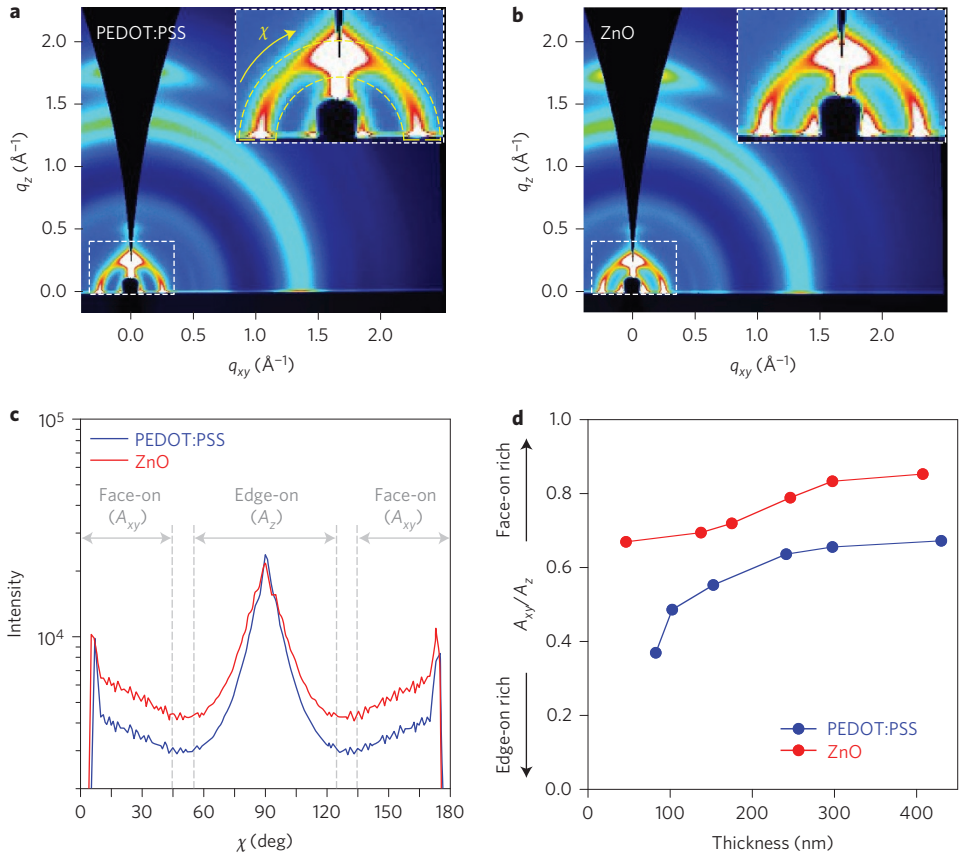

Figure 3 | GIWAXD data for PNTz4T/$PC_{61}BM$ blend films. a, Two-dimensional GIWAXD image of the blend film on the ITO/PEDOT:PSS substrate (thickness, 241 nm). **b**, Two-dimensional GIWAXD image of the blend film on the ITO/ZnO substrate (thickness, 246 nm). Insets: close-up of the lamellar, (100), diffraction region. **c**, Pole figures extracted from the lamellar diffraction for the blend films on both ITO/PEDOT:PSS and ITO/ZnO substrates. Definitions of the polar angle (χ) range corresponding to the edge-on (A_z) and face-on (A_{xy}) crystallites are shown. **d**, Dependence of A_{xy}/A_z on film thickness, where A_{xy}/A_z is the ratio of the face-on to edge-on orientation.

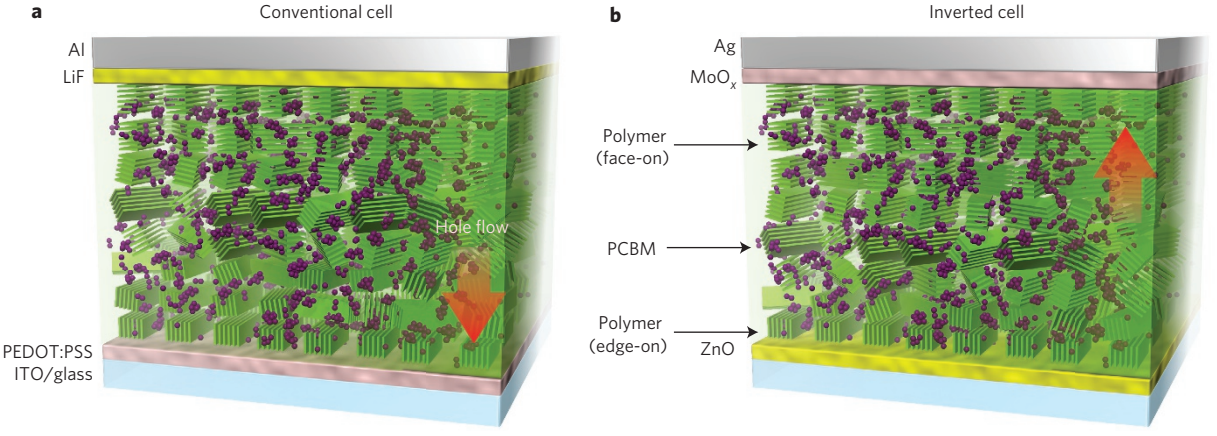

Figure 4 | Schematic illustrations of PNTz4T/$PC_{61}BM$ blend films in the PSCs. a, Conventional cell with PEDOT:PSS as the bottom and LiF as the top interlayer. **b**, Inverted cell with ZnO as the bottom and MoO_x as the top interlayer. The population of face-on crystallite is larger in the inverted cell than in the conventional cell. In both cases, the population of edge-on crystallites is large at the bottom interface and the population of face-on crystallites is large in the bulk through the top interface. Note that the amount of PCBM shown is markedly reduced compared with real cells, and the distribution of the orientation is exaggerated in order to better visualize the polymer orientation.

In regioregular poly(3-hexylthiophene) films it has been reported previously that edge-on crystallites exist at the film–bottom layer interface and that face-on crystallites exist in the bulk and at the film–air interface[38,39]. Thus, in the case of PNTz4T, a class of polythiophene-based polymer, it is natural to consider that the edge-on crystallites are abundant at the film–bottom layer interface and that the face-on crystallites are abundant in the bulk through the film–air interface, regardless of the substrate. The PNTz4T/$PC_{71}BM$ blend film provided similar results to the PNTz4T/$PC_{61}BM$ blend film (Supplementary Figs 14, 15, 17 and 18).

Discussion

We discuss herein the rationale for the markedly high performance of PNTz4T-based cells fabricated using a thicker active layer with the inverted architecture. We assume that the high FF and thus the high efficiency observed, even with thicker films, can be attributed to the quite high vertical hole transport of the polymer ($\mu_h = 2–3 \times 10^{-3}$ cm^2 V^{-1} s^{-1})[20,28,29] and the well-balanced hole and electron transport. The high vertical hole transport apparently originates in the highly crystalline structure with short π–π stacking distance and the face-on orientation.

It has been reported by several groups that the vertical phase gradation of the polymer and PCBM, which is characterized by polymer enrichment at the film–top interlayer (film–air) interface and PCBM enrichment at the film–bottom interlayer interface, is responsible for the increased performance in inverted cells[31,32]. However, energy-dispersive X-ray spectroscopy (EDS) of the cross-section revealed that in all the PNTz4T cells the sulphur content increased weakly from the film–top interface to the film–bottom interface (Supplementary Fig. 21). This suggests that the polymer is weakly but gradually enriched towards the film–bottom layer interface. This 'reverse' vertical polymer concentration gradation should be disadvantageous for the inverted architecture.

Instead, we found that PNTz4T shows a higher tendency to form the favourable face-on orientation on the ZnO surface than on the PEDOT:PSS surface (corresponding to the inverted and conventional cells, respectively). It is also important to mention that we observed unevenly distributed polymer orientations through the film thickness, as revealed by the in-depth GIWAXD studies. The population of the face-on crystallites is larger in the bulk through the film–top interlayer interface, that is, the film–LiF (conventional cell) or MoO_x (inverted cell) top interfaces, and the population of the edge-on crystallites is larger at the film–bottom interlayer interface, that is, the film/PEDOT:PSS (conventional cells) or film–ZnO (inverted cells) interfaces, as shown in Fig. 4. Therefore, in conventional cells, where the generated holes flow towards the bottom PEDOT:PSS layer through the edge-on-rich region, this distribution of the polymer orientation should be detrimental to vertical hole transport, resulting in inefficient hole collection. In contrast, in the inverted cells, where the holes flow towards the top MoO_x layer through the face-on-rich region, this polymer orientation distribution would facilitate vertical hole transport, leading to efficient hole collection. This model is in good agreement with the high J_{SC} and FF, as well as reduced charge recombination, in the inverted cell compared with the conventional cell.

Conclusions

We have demonstrated PCE values reaching 10% in single-junction PSCs with an inverted architecture, using PNTz4T as the p-type material and $PC_{71}BM$ as the n-type material. Notably, these results have been achieved using a thick active layer measuring ~300 nm, which is far thicker than the typical thickness for PSCs and is beneficial for practical use[26,28]. The high efficiency is most probably due to the highly ordered polymer structure in the active layer, in which a highly crystalline structure with short π–π stacking distance and the favourable face-on orientation are achieved. Importantly, we have found that polymer crystallites with face-on orientation are present in greater abundance on the ZnO surface than on the PEDOT:PSS surface, and that the face-on orientation is enriched in the bulk and at the top contact, and the edge-on orientation is enriched at the bottom contact. These unique characteristics in the backbone orientation would facilitate charge transport and reduce charge recombination, particularly in the inverted architecture, resulting in higher J_{SC} and FF. These results are evidence of the great promise of PSCs and indicate that even higher PCEs should be realized by careful molecular design using the NTz moiety.

Methods

Methods and any associated references are available in the online version of the paper.

Received 23 December 2014; accepted 20 April 2015; published online 25 May 2015

References

1. Yu, G., Gao, J., Hummelen, J. C., Wudl, F. & Heeger, A. J. Polymer photovoltaic cells: enhanced efficiencies via a network of internal donor–acceptor heterojunctions. *Science* **270,** 1789–1791 (1995).
2. Günes, S., Neugebauer, H. & Sariciftci, N. S. Conjugated polymer-based organic solar cells. *Chem. Rev.* **107,** 1324–1338 (2007).
3. Brabec, C., Dyakonov, V. & Scherf, U. *Organic Photovoltaics: Materials, Device Physics, and Manufacturing Technologies* (Wiley-VCH, 2008).
4. He, Z. *et al.* Enhanced power-conversion efficiency in polymer solar cells using an inverted device structure. *Nature Photon.* **6,** 591–595 (2012).
5. Ye, L., Zhang, S., Zhao, W., Yao, H. & Hou, J. Highly efficient 2D-conjugated benzodithiophene-based photovoltaic polymer with linear alkylthio side chain. *Chem. Mater.* **26,** 3603–3605 (2014).
6. Liao, S.-H. *et al.* Single junction inverted polymer solar cell reaching power conversion efficiency 10.31% by employing dual-doped zinc oxide nano-film as cathode interlayer. *Sci. Rep.* **4,** 6813 (2014).
7. Liu, Y. *et al.* Aggregation and morphology control enables multiple cases of high-efficiency polymer solar cells. *Nature Commun.* **5,** 5293 (2014).
8. You, J. *et al.* A polymer tandem solar cell with 10.6% power conversion efficiency. *Nature Commun.* **4,** 1446 (2013).
9. You, J. *et al.* 10.2% power conversion efficiency polymer tandem solar cells consisting of two identical sub-cells. *Adv. Mater.* **25,** 3973–3978 (2013).
10. Scharber, M. C. *et al.* Design rules for donors in bulk-heterojunction solar cells—towards 10% energy-conversion efficiency. *Adv. Mater.* **18,** 789–794 (2006).
11. Facchetti, A. π-Conjugated polymers for organic electronics and photovoltaic cell applications. *Chem. Mater.* **23,** 733–758 (2011).
12. Boudreault, P.-L. T., Najari, A. & Leclerc, M. Processable low-bandgap polymers for photovoltaic applications. *Chem. Mater.* **23,** 456–469 (2011).
13. Beaujuge, P. M. & Fréchet, J. M. J. Molecular design and ordering effects in π-functional materials for transistor and solar cell applications. *J. Am. Chem. Soc.* **133,** 20009–20029 (2011).
14. Mühlbacher, D. *et al.* High photovoltaic performance of a low-bandgap polymer. *Adv. Mater.* **18,** 2884–2889 (2006).
15. Peet, J. *et al.* Efficiency enhancement in low-bandgap polymer solar cells by processing with alkane dithiols. *Nature Mater.* **6,** 497–500 (2007).
16. Blouin, N. *et al.* Toward a rational design of poly(2, 7-carbazole) derivatives for solar cells. *J. Am. Chem. Soc.* **130,** 732–742 (2008).
17. Park, S. H. *et al.* Bulk heterojunction solar cells with internal quantum efficiency approaching 100%. *Nature Photon.* **3,** 297–302 (2009).
18. Liang, Y. *et al.* Development of new semiconducting polymers for high performance solar cells. *J. Am. Chem. Soc.* **131,** 56–57 (2009).
19. Liang, Y. *et al.* Highly efficient solar cell polymers developed via fine-tuning of structural and electronic properties. *J. Am. Chem. Soc.* **131,** 7792–7799 (2009).
20. Liang, Y. *et al.* For the bright future—bulk heterojunction polymer solar cells with power conversion efficiency of 7.4%. *Adv. Mater.* **22,** E135–E138 (2010).
21. Mataka, S. *et al.* Sulfur nitride in organic chemsitry. XIV, Selective formation of benzo-and benzobis[1, 2, 5]thiadiazole skeleton in the reaction of tetrasulfur tetranitride with naphthalenols and related compounds. *Bull. Chem. Soc. Jpn* **64,** 68–73 (1991).
22. Wang, M. *et al.* A donor–acceptor conjugated polymer based on naphtho[1,2-*c*:5,6-*c*]bis[1,2,5]thiadiazole for high performance polymer solar cells. *J. Am. Chem. Soc.* **133,** 9638–9641 (2011).
23. Osaka, I. *et al.* Synthesis, characterization, and transistor and solar cell applications of a naphthobisthiadiazole-based semiconducting polymer. *J. Am. Chem. Soc.* **134,** 3498–3507 (2012).
24. Szarko, J. M. *et al.* When function follows form: effects of donor copolymer side chains on film morphology and BHJ solar cell performance. *Adv. Mater.* **22,** 5468–5472 (2010).
25. Guo, X. *et al.* Bithiopheneimide–dithienosilole/dithienogermole copolymers for efficient solar cells: information from structure–property–device performance correlations and comparison to thieno[3,4-*c*]pyrrole-4,6-dione analogues. *J. Am. Chem. Soc.* **134,** 18427–18439 (2012).
26. Peet, J. *et al.* Bulk heterojunction solar cells with thick active layers and high fill factors enabled by a bithiophene-co-thiazolothiazole push–pull copolymer. *Appl. Phys. Lett.* **98,** 043301 (2011).
27. Price, S. C., Stuart, A. C., Yang, L., Zhou, H. & You, W. Fluorine substituted conjugated polymer of medium band gap yields 7% efficiency in polymer–fullerene solar cells. *J. Am. Chem. Soc.* **133,** 4625–4631 (2011).
28. Li, W. *et al.* Efficient small bandgap polymer solar cells with high fill factors for 300 nm thick films. *Adv. Mater.* 3182–3186 (2013).

29. Osaka, I., Kakara, T., Takemura, N., Koganezawa, T. & Takimiya, K. Naphthodithiophene–naphthobisthiadiazole copolymers for solar cells: alkylation drives the polymer backbone flat and promotes efficiency. *J. Am. Chem. Soc.* **135,** 8834–8837 (2013).
30. Osaka, I., Saito, M., Koganezawa, T. & Takimiya, K. Thiophene–thiazolothiazole copolymers: significant impact of side chain composition on backbone orientation and solar cell performances. *Adv. Mater.* **26,** 331–338 (2014).
31. Xu, Z. *et al.* Vertical phase separation in poly(3-hexylthiophene): fullerene derivative blends and its advantage for inverted structure solar cells. *Adv. Funct. Mater.* **19,** 1227–1234 (2009).
32. Guo, X. *et al.* Polymer solar cells with enhanced fill factors. *Nature Photon.* **7,** 825–833 (2013).
33. Stuart, A. C. *et al.* Fluorine substituents reduce charge recombination and drive structure and morphology development in polymer solar cells. *J. Am. Chem. Soc.* **135,** 1806–1815 (2013).
34. Sirringhaus, H., Brown, P., Friend, R. & Nielsen, M. Two-dimensional charge transport in self-organized, high-mobility conjugated polymers. *Nature* **401,** 685–688 (1999).
35. Baker, J. L. *et al.* Quantification of thin film crystallographic orientation using X-ray diffraction with an area detector. *Langmuir* **26,** 9146–9151 (2010).
36. Rivnay, J., Mannsfeld, S. C. B., Miller, C. E., Salleo, A. & Toney, M. F. Quantitative determination of organic semiconductor microstructure from the molecular to device scale. *Chem. Rev.* **112,** 5488–5519 (2012).
37. Umeda, T., Kumaki, D. & Tokito, S. Surface-energy-dependent field-effect mobilities up to 1 cm^2/Vs for polymer thin-film transistor. *J. Appl. Phys.* **105,** 024516 (2009).
38. Kline, R., McGehee, M. & Toney, M. Highly oriented crystals at the buried interface in polythiophene thin film transistors. *Nature Mater.* **5,** 222–228 (2006).
39. Duong, D. T., Toney, M. F. & Salleo, A. Role of confinement and aggregation in charge transport in semicrystalline polythiophene thin films. *Phys. Rev. B* **86,** 205205 (2012).

Acknowledgements

This research was supported by Grants-in-Aid for Scientific Research from The Ministry of Education, Culture, Sports, Science and Technology (MEXT) (nos. 24685030 and 23245041) and by Precursory Research for Embryonic Science and Technology from the Japan Science and Technology Agency. This work was partly supported by the Nanotechnology Platform Program of MEXT. Two-dimensional GIWAXD experiments were performed at SPring-8 with the approval of the Japan Synchrotron Radiation Research Institute (JASRI, proposal no. 2014A1530). The authors thank K. Tajima of CEMS, RIKEN, for helpful discussions regarding the fabrication of inverted cells and for the contact angle measurement, and K. Higashimine of the Center for Nano Materials and Technology, JAIST, for the EDS measurements. The authors thank Y. Hishikawa of the National Institute of Advanced Industrial Science and Technology (AIST) and H. Tobita of Japan Electrical Safety & Environment Technology Laboratories (JET) for technical discussions about the *J*–*V* measurements. The authors also thank Y. Hishikawa and A. Sasaki for measurement of the cell active area.

Author contributions

K.K. prepared the polymer sample. V.V. and I.O. conceived and designed the solar cell experiments. V.V. and K.K. fabricated the conventional cells and K.K. and T.Ka. fabricated the inverted cells. I.O. and T.Ko. conceived and designed the GIWAXD experiments, and K.K. and T.Ko. conducted them. V.V., K.K. and I.O. prepared the manuscript, and all authors discussed and commented on the manuscript. V.V., I.O., K.T. and H.M. directed the project.

Additional information

Supplementary information is available in the online version of the paper. Reprints and permissions information is available online at www.nature.com/reprints. Correspondence and requests for materials should be addressed to V.V., I.O., K.T. and H.M.

Competing financial interests

The authors declare no competing financial interests.

Methods

Materials. PNTz4T samples were synthesized according to a reported procedure[23]. The molecular weights (M_n) of the samples were 50–60 kDa, and the polydispersity index (PDI) was ~2.5. $PC_{61}BM$ and $PC_{71}BM$ were purchased from Frontier Carbon Corporation, Solenne BV and Luminescent Technology Corporation. $PC_{61}BM$s and $PC_{71}BM$s from different suppliers gave similar results. PEDOT:PSS (Clevios P VP Al 4083) was purchased from Heraeus. The patterned ITO-coated glass substrates were purchased from Atsugi Micro.

Thin film characterization. GIWAXD experiments were conducted at SPring-8 on beamline BL46XU. The sample was irradiated with an X-ray energy of 12.39 keV ($\lambda = 1$ Å) at a fixed incident angle on the order of 0.12° through a Huber diffractometer. The GIWAXD patterns were recorded with a two-dimensional image detector (Pilatus 300K). Energy-dispersive X-ray spectroscopy was performed with an atomic-resolution analytical electron microscope (JEOL, JEM-ARM200F).

Solar cell fabrication and characterization. ITO substrates were pre-cleaned sequentially by sonicating in a detergent bath, then with deionized water, acetone and isopropanol at room temperature and in a boiled isopropanol bath, each for 10 min. The substrates were subjected to ultraviolet/ozone treatment at room temperature for 20 min. For conventional cells, the pre-cleaned ITO substrates were coated with PEDOT:PSS by spin-coating (5,000 r.p.m. for 30 s, thickness of ~30 nm) and then baked at 120 °C for 15 min in air. The active layer was deposited in a glove box by spin-coating hot (100 °C) DCB solution containing PNTz4T and $PC_{61}BM$ or $PC_{71}BM$ with a weight ratio of 1:2 at 600 r.p.m. for 20 s. The active layer thickness was controlled by changing the concentration of the solution; for example, an 8 g l^{-1} solution (based on polymer concentration) typically gave an active layer of 250–300 nm thickness. The thin films were transferred into a vacuum evaporator connected to the glove box, and LiF (0.8 nm) and Al (100 nm) were deposited sequentially through a shadow mask under ~10^{-5} Pa, with an active area of the cells of 0.16 cm^2. For the inverted cells, the pre-cleaned ITO substrates (masked at the electrical contacts) were coated with ZnO precursor by spin-coating (3,000 r.p.m. for 30 s) a precursor solution prepared by dissolving zinc acetate dehydrate (0.5 g) and ethanolamine (0.14 ml) in 5 ml 2-methoxyethanol. They were then baked in air at 200 °C for 30 min, then rinsed with acetone and isopropanol, and dried in a glove box. The active layer was deposited as described above. MoO_x (7.5 nm) and Ag (100 nm) were deposited sequentially by thermal evaporation under ~10^{-5} Pa.

The J–V characteristics of the cells were measured with a Keithley 2400 source measure unit in a nitrogen atmosphere under 1 sun (AM1.5G) conditions using a solar simulator (SAN-EI Electric, XES-40S1, 1,000 W m^{-2}). More than 20 cells were analysed to provide average efficiencies for the optimized cells. The cell data obtained when using a photomask (0.1225 cm^2) were consistent with those without the photomask (Supplementary Fig. 5 and Supplementary Table 5). No hysteresis was observed in the J–V curves (Supplementary Fig. 6). PNTz4T/$PC_{71}BM$ cells were also characterized at the Japan Electrical Safety & Environment Technology Laboratories (JET) (Supplementary Fig. s7). The light intensity for the J–V measurements was calibrated with a reference photovoltaic cell (Konica Minolta AK-100, certified by the National Institute of Advanced Industrial Science and Technology, Japan). EQE spectra were measured with a spectral response measuring system (Soma Optics, S-9241). The thickness of the active layer was measured with an AlphaStep D-100 surface profiler (KLA Tencor).

Hole-only and electron-only device fabrication and measurement. For hole-only devices, the pre-cleaned ITO substrates were coated with PEDOT:PSS by spin-coating (5,000 r.p.m. for 30 s, thickness of ~30 nm)[40]. The PNTz4T film or the PNTz4T/$PC_{61}BM$ or $PC_{71}BM$ (1:2 weight ratio) blend film was then spin-coated from a hot (100 °C) DCB solution (8 g l^{-1}, based on polymer concentration) at 600 r.pm. for 20 s. The thin films were transferred into a vacuum evaporator connected to the glove box, and MoO_x (7.5 nm) and Ag (100 nm) were deposited sequentially through a shadow mask. For electron-only devices, the pre-cleaned ITO substrates were coated with ZnO and then with the PNTz4T/$PC_{61}BM$ or $PC_{71}BM$ (1:2 weight ratio) blend film as described above. LiF (2 nm) and Al (100 nm) were deposited sequentially. The J–V characteristics were measured in the range of 0–7 V using a Keithley 2400 source measure unit under nitrogen in the dark, and the mobility was calculated by fitting the J–V curves to a space charge limited current model described by

$$J = (8/9)\varepsilon_r\varepsilon_0\mu(V^2/L^3)$$

where ε_r is the dielectric constant of the polymer, ε_0 is the permittivity of free space, μ is the mobility, $V = V_{appl} - V_{bi}$, where V_{appl} is the applied voltage to the device and V_{bi} is the built-in voltage due to the difference in workfunction of the two electrodes (determined to be 0.1 for the hole-only device and 0.1 for the electron-only device), and L is the polymer thickness. The dielectric constant ε_r is assumed to be 3, which is a typical value for semiconducting polymers.

References

40. Shrotriya, V., Yao, Y., Li, G. & Yang, Y. Effect of self-organization in polymer/fullerene bulk heterojunctions on solar cell performance. *Appl. Phys. Lett.* **89,** 063505 (2006).